2000

Doppler Estimation Using a Coherent Ultrawide-Band Random Noise Radar

Ram M. Narayanan
University of Nebraska-Lincoln

Muhammad Dawood
University of Nebraska-Lincoln

Doppler Estimation Using a Coherent Ultrawide-Band Random Noise Radar

Ram M. Narayanan, *Senior Member, IEEE,* and Muhammad Dawood, *Student Member, IEEE*

***Abstract*—The University of Nebraska has developed an ultrawide-band (UWB) coherent random noise radar operating over the 1–2 GHz frequency range. The system achieves phase coherence by using heterodyne correlation of the received signal with a time-delayed frequency-shifted replica of the transmit waveform. Knowledge of the phase of the received signal and its time dependence due to target motion permits the extraction of the mean Doppler frequency from which the target speed can be inferred. Theoretical analysis, simulation studies, and laboratory measurements using a microwave delay line showed that it was possible to estimate the Doppler frequency from targets with linear as well as rotational motion. Field measurements using a photonic delay line demonstrated the success of this technique at a range of about 200 m at target speeds of up to 9 m/s. Analysis shows that the accuracy with which the Doppler frequency can be estimated depends not only on the phase performance of various components within the system, but also upon the random nature and bandwidth (BW) of the transmit waveform, and the characteristics of unsteady target motion.**

***Index Terms*—Doppler estimation, random noise radar, ultrawide-band radar.**

I. Introduction

DOPPLER radars estimate target velocity by measuring the frequency shift between the transmit and receive frequencies. Thus, these systems can be used to identify moving targets and separate these from stationary targets and slowly varying clutter. These systems maintain phase coherence by using the same stable master oscillator (STAMO) for mixing and frequency conversion in the transmitter and the receiver.

The University of Nebraska, Lincoln, has developed a technique that succeeds in injecting coherence in a radar system that transmits wide-band random noise. Phase coherence is obtained using heterodyne correlation of the received signal with a time-delayed frequency-translated replica of the transmit waveform. This ensures that the reflected signal, when mixed with the time-delayed transmit signal, yields the same intermediate frequency, thereby preserving the phase contained within the reflected signal. This system operates over 1–2 GHz frequency band, thereby achieving 1-GHz instantaneous bandwidth yielding a down-range resolution of 15 cm. The phase coherence in the system has been used to configure the radar as a Doppler radar for measurement of target velocity, the results of which are described in this paper.

Manuscript received June 24, 1999; revised February 25, 2000. This work was supported by the Office of Naval Research under Contract N00014-1-97-0200.

The authors are wih the Department of Electrical Engineering, Center for Electro-Optics, University of Nebraska, Lincoln, NE 68588-0511 USA.

Publisher Item Identifier S 0018-926X(00)05803-8.

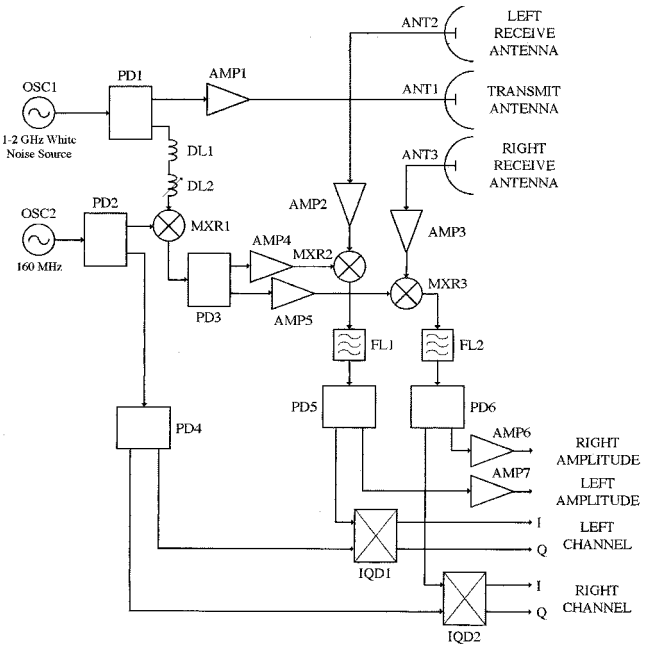

Fig. 1. Block diagram of ultrawide-band random noise radar system.

Section II provides a description of the University of Nebraska's 1–2 GHz coherent random noise radar system. In Section III, we develop the basic theory of Doppler estimation using the system. Results of computer simulations are shown in Section IV, which support the theoretical analysis. Experimental results for the short-range laboratory measurments and the long-range field measurements are shown in Sections V and VI, respectively. An analysis of error sources and their effects on Doppler performance is provided in Section VII. Section VIII provides a discussion of the results and presents conclusions.

II. Description of Coherent Random Noise Radar System

A block diagram of the polarimetric random noise radar system is shown in Fig. 1 [1]. This system was originally designed to detect and identify shallow buried objects, such as landmines. The noise signal is generated by a noise source OSC1, which provides a wide-band noise signal with a Gaussian amplitude distribution and a constant power spectral density in the 1–2-GHz frequency range, with a power output of 0 dBm. This output is split into two in-phase components in power divider PD1. One of these outputs is amplified in a 34-dB gain power amplifier AMP1, which has a 1-dB gain compression point greater than +40 dBm. Thus, the average power output of AMP1 is +30 dBm (1 W), but the amplifier

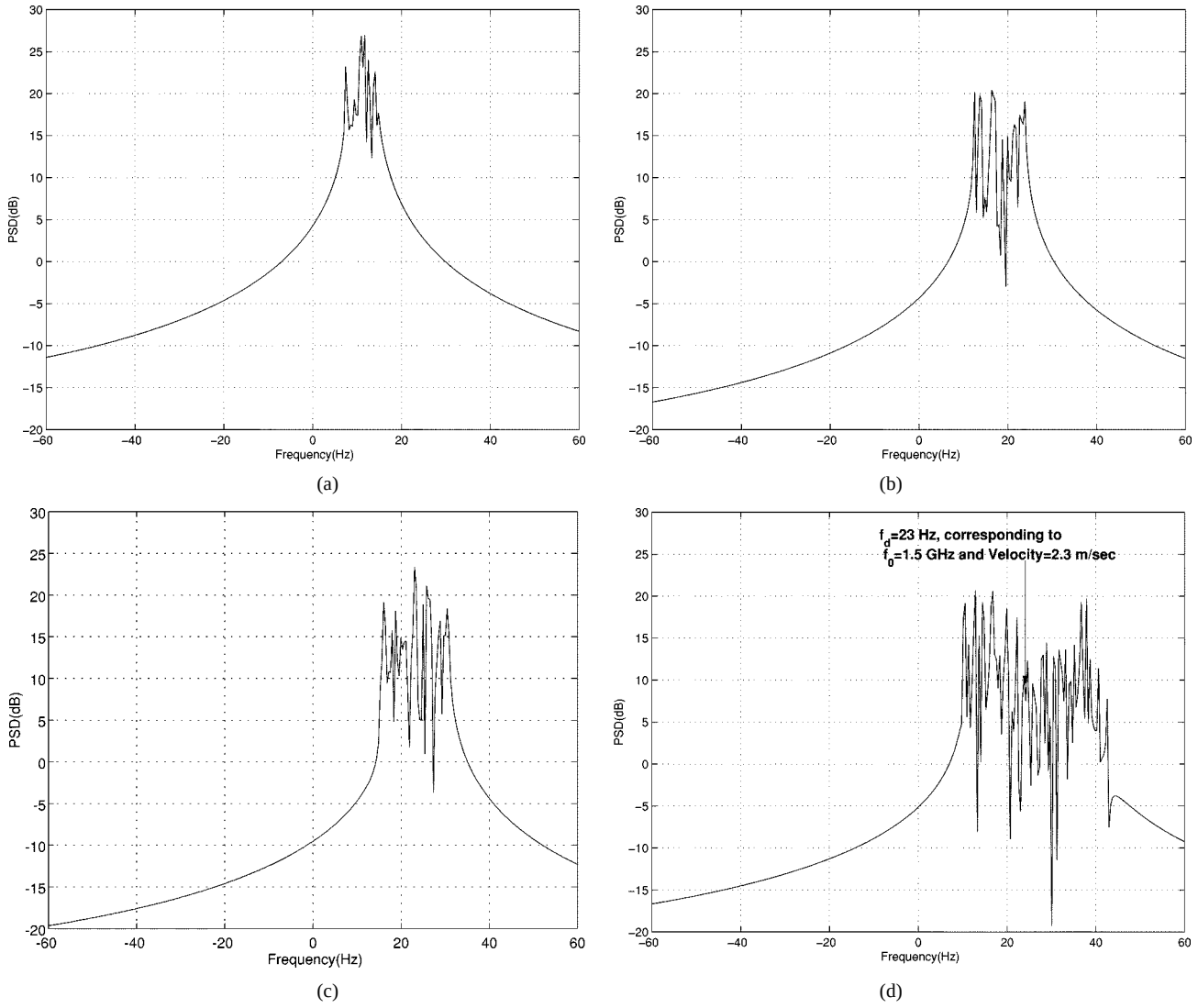

Fig. 2. Simulated Doppler spectra of linear motion at velocities of (a) 1.1 m/s; (b) 1.8 m/s; (c) 2.3 m/s; and (d) 2.3 $\pm$ 1 m/s.

is capable of faithfully amplifying noise spikes that can be as high as 10 dB above the mean noise power. The output of the amplifier is connected to a broad-band (1–2 GHz) transmit horn antenna ANT1. The E/H plane beamwidths and gain of ANT1 at the center frequency of 1.5 GHz are 23°, 34°, and 17 dB, respectively.

The other output of the power divider PD1 is fed to a combination of a fixed and variable delay lines: DL1 and DL2, respectively. These delay lines are used to provide the necessary transmit delay so that it can be correlated with the received signal scattered from objects at appropriate distance corresponding to the delay. The variable delay line is a seven-bit programmable stepped delay line that can be varied from 0 to 19.812 ns in 0.156 ns steps. The fixed delay line is physically realized by a low-loss linear phase shifter in the 1–2 GHz frequency range.

In order to perform coherent processing of the noise signals, the delayed replica of the transmit waveform is mixed in MXR1 with an IF signal produced by a 160-MHz phase-locked oscillator OSC2, which is phase-locked to an internal 1–5 MHz crystal. MXR1 is a lower side-band upconverter that yields an output within the 0.84–1.84-GHz frequency range, while the upper side-band output at 1.16–2.16 GHz is internally terminated. This coherent noise signal is split by power divider PD3 into two identical channels, which can also be configured as the copolarized and the cross-polarized channels.

We will now discuss the signal processing of one of the channels since other channel operation is essentially identical. One of the outputs of PD3 is amplified in AMP4, a 19-dB gain amplifier. Since this signal is noiselike, amplifier AMP4 is chosen so as to provide a linear output of $+10$ dBm minimum. This signal is used as the local oscillator (LO) input to a biasable mixer, MXR2, whose RF input is obtained from receive antenna ANT2 and a 20-dB gain low-noise amplifier AMP2. The receive antenna is a dual-polarized log-periodic antenna of constant 7.5 dB gain over the 1- to 2-GHz frequency range. Amplifier AMP2 is used to improve the receiver noise figure. Mixer MXR2 is dc-biased in the square-law region, which ensures that the mixing process is efficient for low LO drive levels. In general, the RF input signal to mixer MXR2 consists of transmitted noise at 1–2 GHz scattered and reflected from various targets. However, since the LO signal has a unique delay associated with it, only

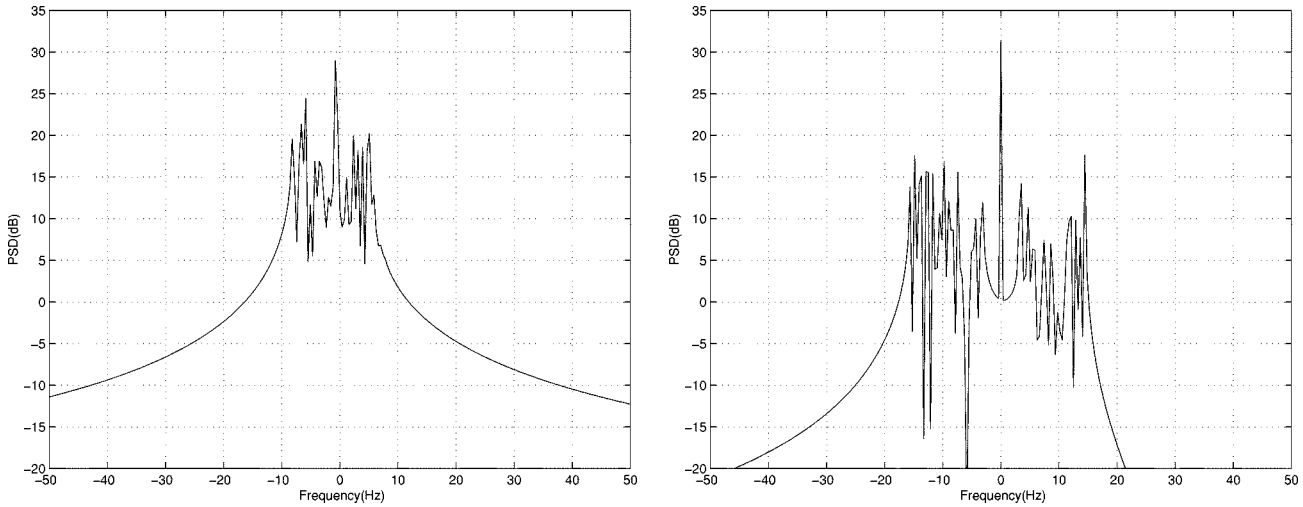

(a) (b)

Fig. 3. Simulated Doppler spectra of rotating target at (a) 40 rpm and (b) 75 rpm.

the signal scattered from the appropriate range bin will mix with the LO to yield an IF signal at 160 MHz. Signals scattered or reflected from other range bins, will not be correlated with the delayed replica. The output of the mixer MXR2 is connected to a narrow-band bandpass filter FL1 of center frequency 160 MHz and bandwidth 5 MHz, ensuring that only 160-MHz signals get through. The output of filter FL1 at 160 MHz is split into two equal outputs by power divider PD5. One of these outputs is amplified and detected in a 70-dB dynamic range 160-MHz logarithmic amplifier AMP6 of 20-MHz bandwidth. The other output of power divider PD5 is connected to one of the inputs of I/Q detector IQD1, whose reference frequency input is one of the outputs from PD4. Both of the signals are centered at 160 MHz; thus, the I/Q detector provides the in-phase (I) and quadrature (Q) components of the two signals. Since frequency translation preserves phase differences, the I and Q outputs can be used to extract the Doppler shift produced due to the motion of the target.

If the radar system is configured in both copolarized and cross-polarized modes, it will produce the following outputs at various ranges as set by the delay lines: 1) copolarized amplitude; 2) copolarized phase angle; 3) cross-polarized amplitude; and 4) cross-polarized phase angle. The system outputs can, therefore, be related to the polarimetric scattering characteristics of the target besides Doppler estimation.

III. Theory of Doppler Estimation Using Coherent Random Noise Radar

Since the transmitted amplitude has a Gaussian amplitude distribution and uniform power spectral density, it can be modeled as

$$v_t(t) = a(t)\cos\{(\omega_0 \pm \delta\omega)\,t + \psi_t\} \tag{1}$$

where $a(t)$ represents the Gaussian amplitude distribution, $(\omega_0/2\pi)$ is the center frequency at 1.5 GHz, $(\delta\omega/2\pi)$ is uniformly distributed over the $\pm$0.5-GHz frequency range, and ψ_t is the arbitrary transmitter phase.

The time-delayed version of the transmitted signal $v_t(t)$ is mixed in MXR1 with the reference frequency $(\omega_{ref}/2\pi)$ at 160 MHz to produce the lower side-band output $v_{m1}(t)$ given by

$$v_{m1}(t) = k_1 a(t-\tau)\cos\{(\omega_0 \pm \delta\omega - \omega_{ref})\,(t-\tau)\} \tag{2}$$

where k_1 is some constant and τ is the delay.

The echo from the target is expressed as

$$v_r(t) = k_2 a(t)\rho\cos\left\{(\omega_0 \pm \delta\omega)\left(t - \frac{2R}{c}\right) + \psi_t + \psi_s\right\} \tag{3}$$

where c is the velocity of light, ρ and ψ_s are the amplitude and phase of the target reflectivity, and the term $2R/c$ represents the time taken by the transmitted wave to return to the receiver from the target at range R.

The instantaneous phase of the echo voltage can be defined as

$$\psi_r = \left(\frac{-4\pi R}{\lambda}\right) + \psi_t + \psi_s \tag{4}$$

where

$$\lambda = \frac{c}{f_o \pm \delta f} \tag{5}$$

is the instantaneous wavelength.

If the target is in motion, ψ_r will change with time and (3) can be written as

$$v_r(t) = k_2 a(t)\rho\cos\left\{\left(\omega_o \pm \delta\omega - \frac{4\pi V}{\lambda}\right)t + \psi_t + \psi_s\right\} \tag{6}$$

where V is the target velocity given by dR/dt, and k_2 is a constant.

This received echo is mixed with the output of MXR1 at a delay time set equal to $2R/c$, yielding

$$v_{m2}(t) = k_3\rho a^2(t)\cos\left\{\left(\omega_{ref} - \frac{4\pi V}{\lambda}\right)t + \psi_s\right\} \tag{7}$$

where k_3 is some constant.

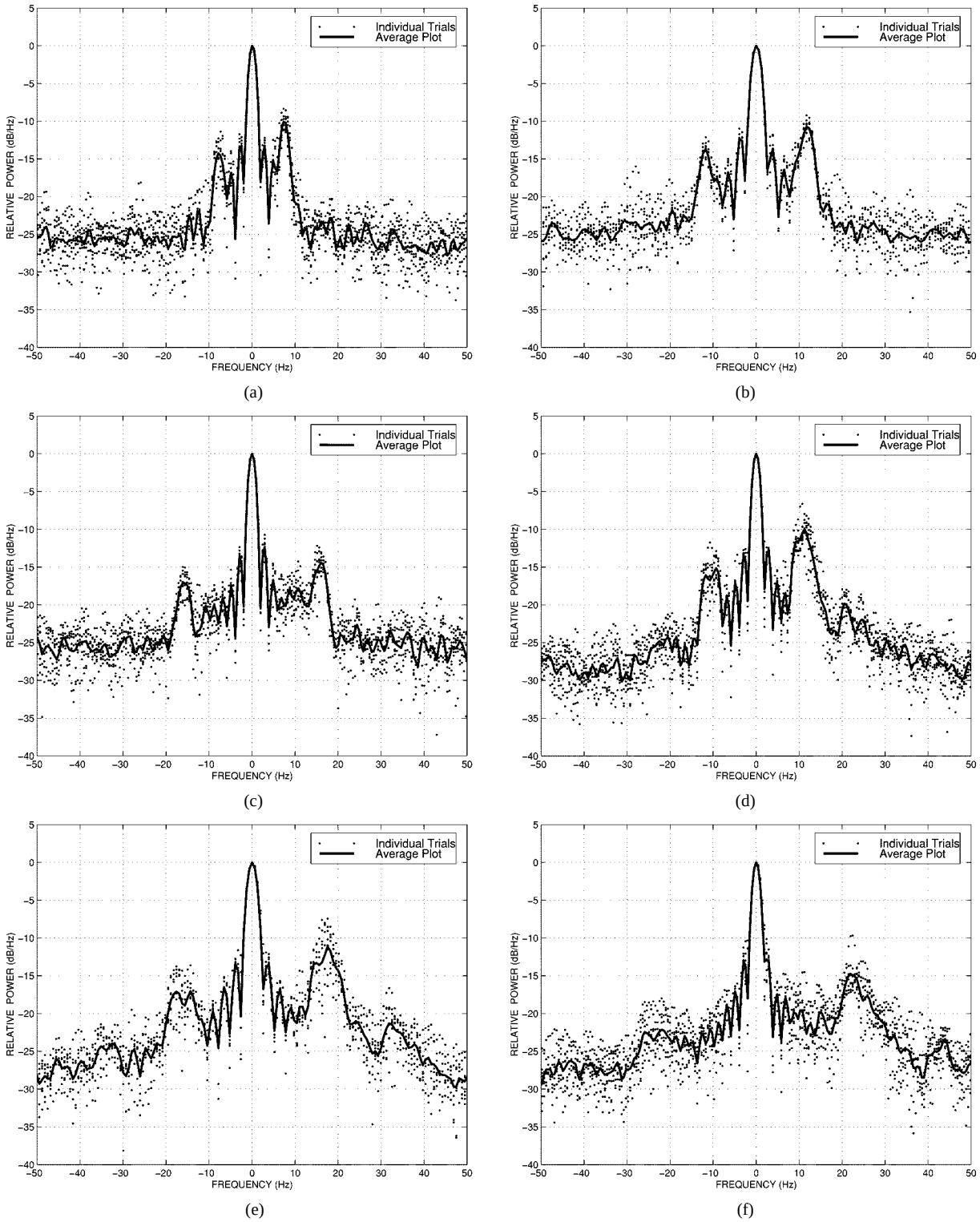

Fig. 4. Measured Doppler spectra of linear motion at short range at 1-GHz fixed frequency for velocities of (a) 1.1 m/s; (b) 1.8 m/s; and (c) 2.3 m/s; also, at 1–2 GHz random frequency for velocities of (d) 1.1 m/s; (e) 1.8 m/s; and (f) 2.3 m/s.

The output of MXR2 and ω_{ref} are fed to the I/Q detector producing inphase and quadrature components that are proportional to the cosine and sine of the phase difference, respectively

$$I = k_I \cos\left\{-\frac{4\pi V}{\lambda}\, t + \psi_s\right\} \tag{8}$$

$$Q = -k_Q \sin\left\{-\frac{4\pi V}{\lambda}\, t + \psi_s\right\} \tag{9}$$

where k_I and k_Q represent the amplitudes of the I and Q components, respectively. We note that the I and Q outputs are time-varying functions depending upon the target velocity V. The Doppler frequency f_d is given by $(1/2\pi)$ times the total phase and can be shown to be equal to

$$f_d = -\frac{2V}{\lambda}. \tag{10}$$

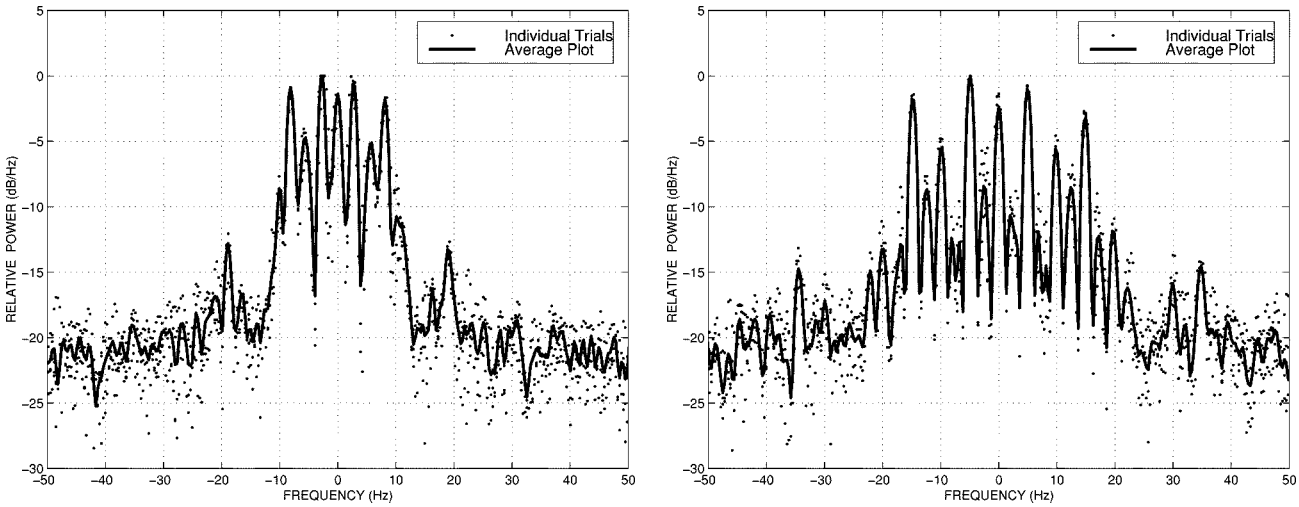

(a) (b)

Fig. 5. Measured Doppler spectra for rotating targets at (a) 40 rpm and (b) 75 rpm.

In the above equation, the negative sign appears due to the fact that a positive radial velocity generates a negative Doppler shift and is associated with an outward moving target. However, the combination $I + jQ$ will generate a positive or negative Doppler shift for an outward or inward moving target, respectively, due to the negative sign appearing in (9). Note that the instantaneous Doppler frequency is not a constant but varies due to the varying nature of the instantaneous wavelength λ. Since λ varies between $\lambda_{\min}$ (0.15 m) and $\lambda_{\max}$ (0.3 m) corresponding to a frequency variation between $f_{\min}$ (1 GHz) and $f_{\max}$ (2 GHz), the Doppler frequencies vary from f_{dl} to f_{dh}. The relationship between f_{dl}, f_{dh}, and f_{d0}, the mean Doppler corresponding to transmit frequency of $(\omega_0/2\pi) = \frac{f_{\min}+f_{\max}}{2}$ (1.5 GHz) can be shown to be

$$f_{dl} = \frac{2f_{\min}f_{d0}}{f_{\min}+f_{\max}} \quad \text{and} \quad f_{dh} = \frac{2f_{\max}f_{d0}}{f_{\min}+f_{\max}}. \tag{11}$$

Knowing either the minimum or the maximum Doppler frequency, the target velocity V can be computed as

$$V = \frac{cf_{dl}}{2f_{\min}} = \frac{cf_{dh}}{2f_{\max}}. \tag{12}$$

However, in practice, all frequencies in the range of 1–2 GHz are not always present within a finite observation interval. Therefore, it is required that the frequency components be averaged over longer intervals. Since samples are uncorrelated and statistically independent of each other, an average power spectral density $\overline{S(\omega)}$ from N trials can be computed as

$$\overline{S(\omega)} = \frac{1}{N}\sum_{i=1}^{i=N} S_i(\omega) \tag{13}$$

where $S_i(\omega)$ is the power spectral density (PSD) estimate at each frequency per trial, and N is the total number of trials.

This averaging for a transmit waveform centered at f_0 with uniform PSD results in a peak Doppler spectra corresponding to

$$f_{d0} = \frac{-2V}{\lambda_0} \tag{14}$$

where $\lambda_0 = 0.2$ m, corresponding to the mean transmit frequency of 1.5 GHz.

IV. Results of Computer Simulations

Various simulations were performed to evaluate the performance of the radar system. Results of these simulations are shown in Figs. 2 and 3.

In Fig. 2, the simulated Doppler spectra for linear motion are presented. The target is assumed to be moving away from the radar along the boresight direction with constant velocity, i.e., cases (a) 1.1 m/s, (b) 1.8 m/s, (c) 2.3 m/s, and (d) 2.3 $\pm$ 1 m/s. From these figures, it is seen that as the target velocity increases, the Doppler center frequency and spread increase. The spread is symmetric around the center frequency, for a constant target velocity, i.e., cases (a), (b), and (c), and the target velocity can be extracted using (11), (12), and (14). Fig. 2(d) corresponds to a case with nonuniform velocity, which shows that as the target velocity changes, the Doppler spread is asymmetric with respect to the center frequency. However, this asymmetric behavior may or may not be of any significance depending on the type of the target under consideration and the dwell time. The lower cutoff frequency yields information on the minimum speed and the upper cutoff frequency yields information on the maximum speed.

In Fig. 3, the Doppler spectra of a fixed rotating target are presented for 40 rpm and 75 rpm, respectively. The radius of rotation is assumed to be 0.15-m with a 10-cm-long cylindrical target of 5 cm diameter placed at each end. The spectrum contains all frequencies from $-f_{dh}$ to $+f_{dh}$, including frequencies at and close to dc. The outer skirt of the spectra corresponds to the upper limit of the transmitted frequency and provides information on the target's rotational speed if its radius is known. Also, it is seen that as the rotational speed increases, the spectrum correspondingly widens.

The simulation results clearly show the broadening of the Doppler spectra caused by the ultrawide-band nature of the transmit waveform even for a target moving linearly with a uniform velocity. If the target moves with nonuniform velocity around a mean value, additional Doppler spectral broadening occurs. This makes it difficult to separate two or more moving targets at the same time on the basis of their Doppler spectra,

unless they possess no overlap. This effect is more apparent in the Doppler spectra of rotating targets, which may be considered to contain all linear velocities, both positive and negative, between zero and a maximum value given by the product of the radius and the rate of rotation. The Doppler spectra in this case appears as a continuum, with the positive and negative limits being determined by the highest transmit frequency.

V. Results of Short-Range Laboratory Measurements

The results of short-range laboratory measurements carried out using the random noise radar are shown in Figs. 4 and 5. The target moved away from the radar along the boresight direction with approximate uniform velocity, i.e., cases (a) 1.1 m/s, (b) 1.8 m/s, and (c) 2.3 m/s. These targets were small corner reflectors with side lengths of 10 cm. The total range of the radar was subdivided into 22 range bins, each having a resolution of 15 cm and the radar was operated in the 20th range bin. Since a single target passed through a specific range bin very quickly, the number of collected samples were not adequate for meaningful data analysis. To overcome this, a linear array of ten corner reflectors was fabricated on a 0.5-m-long wooden strip, thereby permitting an extended observation time within the range bin. This wooden strip was then used as the target. For comparison purposes and to obtain a good reference, each experiment was also repeated at a fixed 1 GHz transmitted frequency. Furthermore, all experiments were repeated eight times, and their respective PSD's were averaged as shown in (13). The data, about 150–200 points, were acquired by sampling I and Q channels at 500 Hz using a 12-bit A/D data acquisition board. The average PSD was obtained by zero padding the data to 512 points and by using the periodogram technique.

Fig. 4(a)–(c) shows the Doppler spectra of linear motion using the fixed 1-GHz reference frequency at the above three velocities. The respective Doppler components corresponding to these velocities are (a) 7 Hz, (b) 12 Hz, and (c) 15–16 Hz and corresponding calculated target velocities are (d) 1.05 m/s, (e) 1.8 m/s, and (f) 2.3 m/s, respectively. Fig. 4(d)–(f) depict the average Doppler spectra of linear motion using the 1–2 GHz random noise signal at the same respective velocities. The central peaks of the Doppler spectra corresponding to mean transmit frequency of 1.5 GHz are at (d) 11 Hz, (e) 17–18 Hz, and (f) 22–23 Hz. The estimated target velocities corresponding to these Doppler frequencies are 1.1 m/s, 1.8 m/s and 2.3 m/s, respectively. These velocities compare very well with the estimated velocities using a fixed frequency transmission. It may also be noted that we have not suppressed the dc components in these figures.

Fig. 5 shows the Doppler spectra of a rotational target at (a) 40 rpm and (b) 75 rpm. The target was composed of two small 10-cm-long cylinders of 5 cm diameter, which were placed 15 cm from the center of rotation. The results, averaged over four experiments, compare very favorably with the simulated results shown in Fig. 3(a) and (b).

VI. Results of Long-Range Field Measurements

The existing radar system containing the digital delay line DL2 with a maximum delay of approximately 20 ns was modified by adding a fixed photonic delay line of approximately 1.35 μs delay. This delay line was obtained on loan from SPAWAR. The effective range from the antenna of the radar to the target

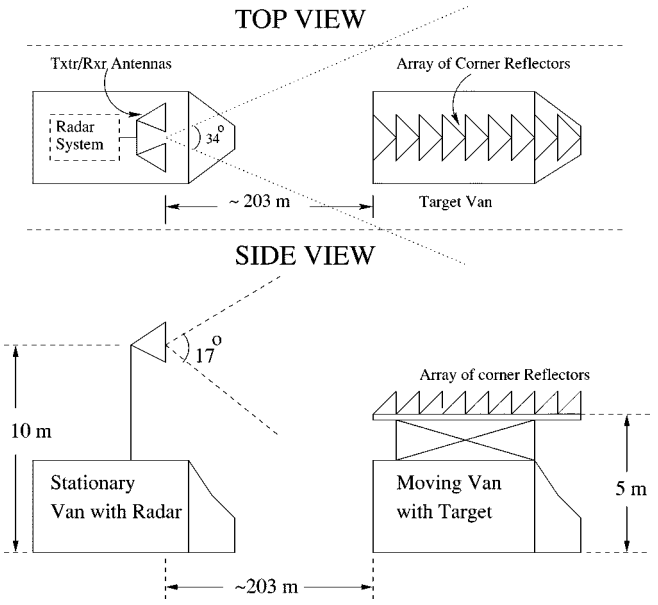

Fig. 6. Geometry of field experiments for Doppler measurements.

(a)

(b)

Fig. 7. Photographs of field measurement setup.

was thus extended to approximately 203 m. The output power of the transmitter was also increased from +30 to +42 dBm using a TWT amplifier to ensure adequate SNR at that range.

A triangular trihedral with 45.7-cm sides was chosen as a target. Since each radar range bin is 15 cm long as a result of the 1-GHz instantaneous transmit bandwidth, a linear array of such triangular trihedrals was assembled on a specifically constructed wooden platform. This wooded structure was mounted at a height of 3 m atop a van. This height was required to minimize the effect of ground multipath interference. However, since the radar was being operated in one range bin of 15 cm width at a time, the interference from the ground did not affect the measurement as it appeared in range bins well removed from the operational range bin. The overall geometry of these experiments is shown in Fig. 6 and a photograph of the field measurement setup is shown in Fig. 7.

The radar system was mounted inside another van, and the antennas were mounted on top of the 10-m-high telescopic boom. The distance between the stationary radar van and the moving target van was approximately 200 m, consistent with the fixed delay line. The field measurements were conducted on a long stretch of abandoned road near Lincoln, NE.

The target van moved away from the radar van along the boresight direction with approximate uniform velocities of 10 miles/hr (4.5 m/s), 15 miles/hr (6.7 m/s), and 20 miles/hr (9 m/s). The Doppler frequencies corresponding to each of these speeds at 1.5-GHz mean frequency are 45, 67.5, and 90 Hz, respectively. In order to compare and contrast the performance of the UWB Doppler radar, each experiment was also repeated at 1.5-GHz fixed frequency and at a random frequency centered at 1.5 GHz with 200-MHz bandwidth. The data were collected in a similar manner as done for the short-range experiments. However, the sampling frequencies ranged from 500 to 1000 Hz corresponding to the abovementioned velocities and data points were zero padded to 1024 points. At each speed, ten trials were carried out and the collected data were analyzed using periodogram technique. The results of these field experiments using the UWB random noise radar are depicted in Figs. 8–10. These figures show the individual trials along with the extracted mean Doppler at each frequency.

It can be concluded from these figures that:

1) the Doppler frequency associated with a moving target can be extracted using the UWB random noise system developed by UNL;
2) the estimated Doppler using a comparatively narrow bandwidth (i.e., 200 MHz) is almost identical to that using a fixed frequency;
3) the Doppler spread increases at higher bandwidths and higher target velocities.

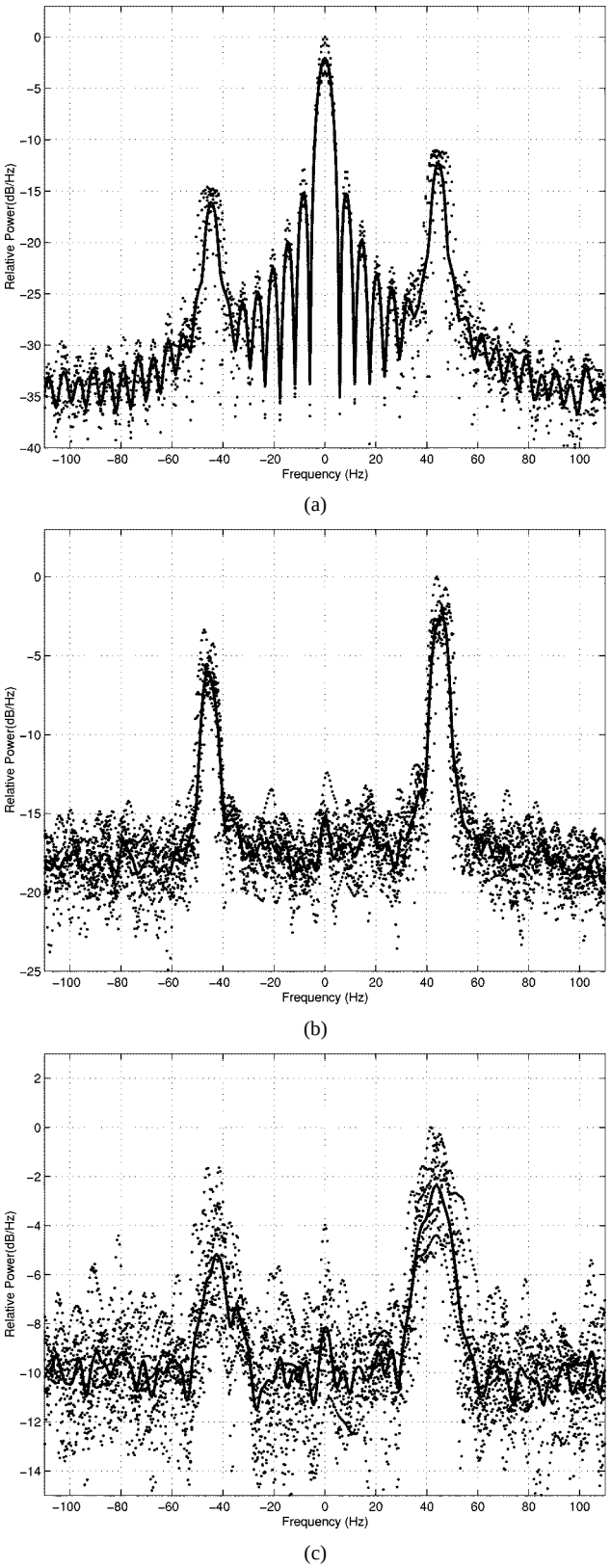

Fig. 8. Measured Doppler spectra of target moving at 4.5 m/s (10 mph) using (a) 1.5-GHz fixed frequency; (b) 1.4–1.6-GHz random frequency; and (c) 1.2-GHz random frequency.

VII. Error Sources and Their Effects

A. System Related Instabilities

In a conventional radar, the primary sources of radar instabilities are usually the stable local oscillator (STALO) or the transmitter. Most modern radars use the STALO to generate the transmitted pulse and to shift the frequency of the received echo. Therefore, the STALO needs to be free of unwanted spurious modulations. Furthermore, any radar that relies upon radial velocity differences between target and clutter must necessarily

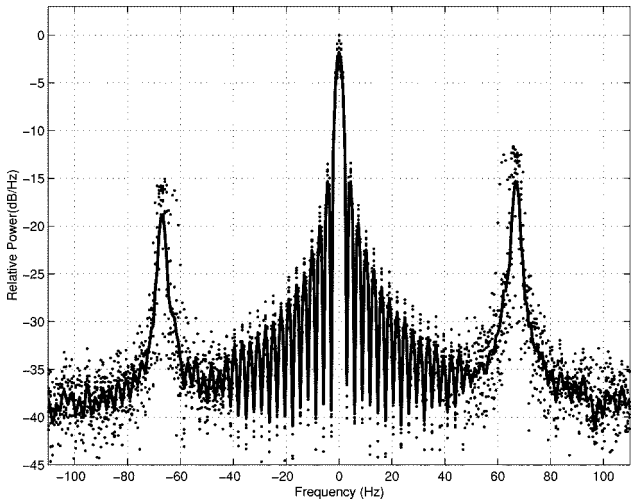

(a)

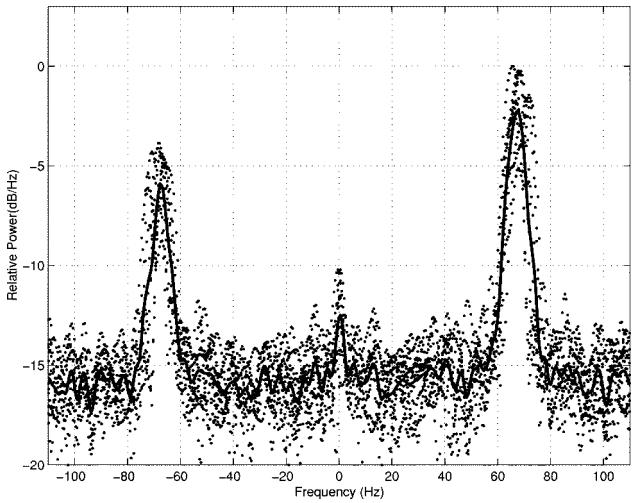

(b)

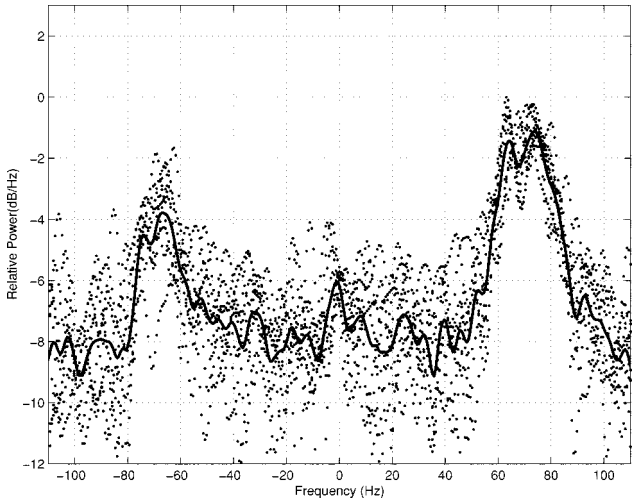

(c)

Fig. 9. Measured Doppler spectra of target moving at 6.7 m/s (15 mph). Same as Fig. 8.

rely on the coherence between the transmitter and the local oscillator. Spurious angle modulation of the transmitter will be transferred to the delayed return from the clutter at an offset frequency equal to the Doppler frequency difference between target and clutter and the side bands from the large clutter will obscure the target signal. Maximum Doppler discrimination can be achieved in a pure CW radar system. Thus, this system has the most demanding requirements for a low level of spurious angle modulation.

In a pure CW system, if the replica of the transmitted signal is mixed with a stable IF oscillator, which is subsequently used for the correlation process, then it can be shown that any spurious phase modulation in the transmitter source can be transferred to the receive chain. The peak phase modulation index of the IF output, $\acute{\theta}(\tau)$ can be shown to be [2]

$$\acute{\theta}(\tau) = \theta_0 2\pi f_n \tau \tag{15}$$

where f_n is the spurious modulating frequency, $\tau(=2R/c)$ is a range related delay, and θ_0 is the transmitter modulation index.

However, if the replica of the transmitted waveform is delayed, then the abovementioned spurious modulation is completely removed due to the correlation process. This is true for our coherent random noise radar and as such no transmitter related stability problem exists in the system.

Other phase nonlinearities and spurious effects in mixers and I/Q detectors that are often noted for conventional radars do affect the UWB noise radar system as well. For example, imbalances in the gain and nonquadrature shift between the I and Q channels create an image spectrum symmetrical to actual spectrum. However, all these nonlinearities can be compensated reasonably well, either using good quality components or through signal processing techniques.

Furthermore, random phase errors may also be contributed by temperature effects and mechanical vibrations. As an example, for a typical slow aircraft with 483 km/hr (300 miles/hr) speed, the requirement to maintain the phase error less than 0.5° at $\lambda = 20$ cm requires that acceleration be maintained below 1000 g. Thus, for a highly agile platform with maximum acceleration of 15 g will yield a negligible phase errors. Similarly, temperature changes that cause slow changes in the path lengths between I and Q channels also contribute errors, but these will be negligible at operating frequency of 1–2 GHz.

B. Uncertainties Caused by Random Nature of Transmit Waveform

The random nature of the transmit waveform has an inherent uncertainty in measuring the Doppler shift, although it can be reduced using a longer observation period. Consider a radar signal that is totally random in nature, specifically white noise. The autocorrelation of such a signal $R_x(\tau)$ centered at frequency f_c can be written as [3]

$$R_x(\tau) = R_c(\tau)\cos(2\pi f_c \tau) \tag{16}$$

where $R_c(\tau)$ is the envelope of the correlation function and is completely determined by the bandwidth and shape of the signal spectrum.

Assume a reference signal $r(t)$, an amplitude-scaled, time-delayed, and time-scaled version of the transmit signal $x(t)$ given as

$$r(t) = x[(1+\alpha_r)t - \tau_r] \tag{17}$$

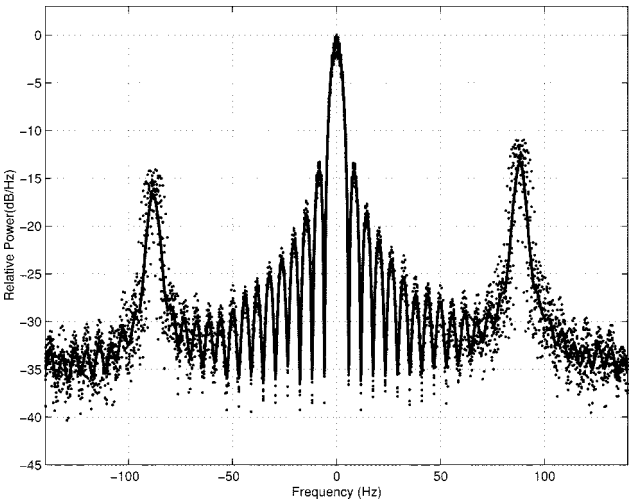

(a)

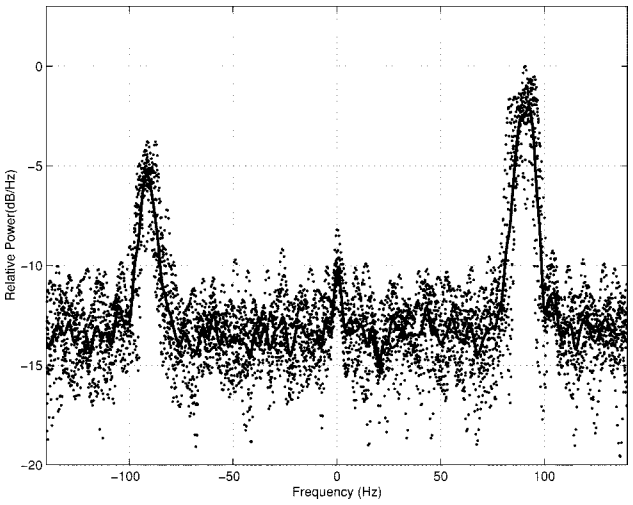

(b)

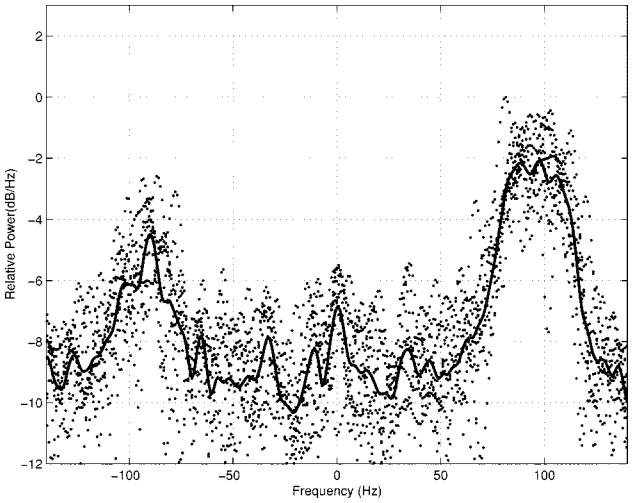

(c)

Fig. 10. Measured Doppler spectra of target moving at 9 m/s (20 mph). Same as Fig. 8.

where $\alpha_r = (2V_r/c - V_r) \simeq (2V_r/c)$, c is velocity of light, V_r is the reference velocity and $\tau_r = (2R/c)$, R being range of the target.

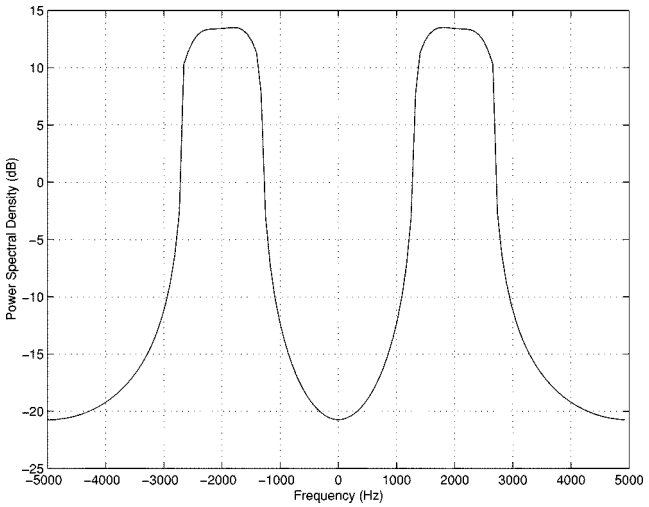

Fig. 11. Doppler spectra of target moving at 200 m/s for uniform power spectral density (PSD) transmit waveform.

The cross-correlation signal R_{yr} between the received signal $y(t)$ and the reference signal $r(t)$ can be expressed as

$$R_{yr} = \sum_{k=1}^{N} a_k R_c[(\alpha_r - \alpha_k)t - (\tau_r - \tau_k)] \cdot \cos(2\pi f_c[(\alpha_r - \alpha_k)t - (\tau_r - \tau_k)]) \quad (18)$$

where a_k is the amplitude of kth scatterer, $\alpha_k \simeq (2V_k/c)$ is the delay rate corresponding to velocity of the kth scatterer, and N is the total number of scatterers.

The central frequency f_c of the transmit waveform can be related to the kth scatterer as follows:

$$(\alpha_r - \alpha_k) f_c = \frac{2(V_r - V_k)}{\lambda_0} \quad (19)$$

where $\lambda_0 = c/f_{d0}$, the radar wavelength at the center frequency.

Assuming a single scatterer at a delay $\tau_r = \tau_k$, reference velocity $V_r = 0$, the spectral density of the Doppler shift corresponding to a transmit waveform of uniform density at a target velocity of 200 m/sec is shown in Fig. 11.

It can easily be seen that due to the transmit nature of the signal, the Doppler frequency f_d is a probabilistic function whose width is governed by the bandwidth of the transmit waveform and target velocity distribution characteristics. Therefore, there exists an inherent uncertainty in measuring the mean Doppler frequency $\overline{f}_d$. This measurement error will be further compounded when the velocity distribution of the target is considered since a practical target usually possesses some deviation about its mean velocity. Since the uncertainty due to transmit waveform and that due to target motion are statistically independent, the total fractional uncertainty $|\delta f/\overline{f}_d|$ can be added in quadrature [4]. Furthermore, the receiver and atmospheric noise will add additional uncertainty in estimating the Doppler shift. However, at higher SNR's it is likely to be below 10% and for a steady target using simulation it is seen to be around 5%.

C. Uncertainties Caused due to Unsteady Target Motion

Target motion cannot generally be approximated by a straight line even if one attempts to fly a straight course, since

air turbulence causes random yaw motion about some mean velocity, thereby, producing Doppler scintillation. Consider a typical wide body rigid frame target moving along a straight path and being influenced by air turbulence. It is reasonable to assume that all angle changes are of random nature that will constitute a Gaussian function. The Doppler distribution has the shape of a modified Hankel function [5] and the standard deviation of angle scintillation, σ_ψ, is an inverse function of transmit wavelength. The overall standard deviation in Doppler as observed at radar will also be influenced by the standard deviation of the aircraft nose-on view profile and wingspan. However, assuming a steady aircraft with air turbulence causing a small deviation, the overall distribution of the Doppler spectrum $S_d(f)$ can be approximated by a Gaussian pdf with small variance, given by

$$S_d(f) = \frac{1}{\sqrt{2\pi}\sigma_\psi(2\sigma_t)} e^{\frac{-(f-f_{d0})^2}{\sigma_\psi^2(2\sigma_t)^2}} \tag{20}$$

where f_{d0} is the mean Doppler frequency and σ_ψ and $2\sigma_t$ are standard deviations of $g(\psi)$ (slope of radar echoes phase front) and $h(t)$ (twice the rate of change of aspect angle with time), respectively.

Such a model has been assumed for estimating Doppler frequencies from random noise radar and fixed frequency radar. Using the approach in [6], noise was introduced in the received waveform and Doppler frequency was estimated at different SNR's and then averaged over 1000 samples. The standard deviation of Doppler estimation at different SNR's for these three cases are shown in Fig. 12. It can be clearly seen in this figure that at low SNR's below 5 dB, the performance of UWB random noise radar is better compared to that of fixed frequency and narrow-band random noise radar. As SNR increases beyond 5 dB, the fractional uncertainty using fixed frequency and narrow-band random noise can be made arbitrarily small; however, for UWB random noise the fractional uncertainty cannot be reduced below 4–5%.

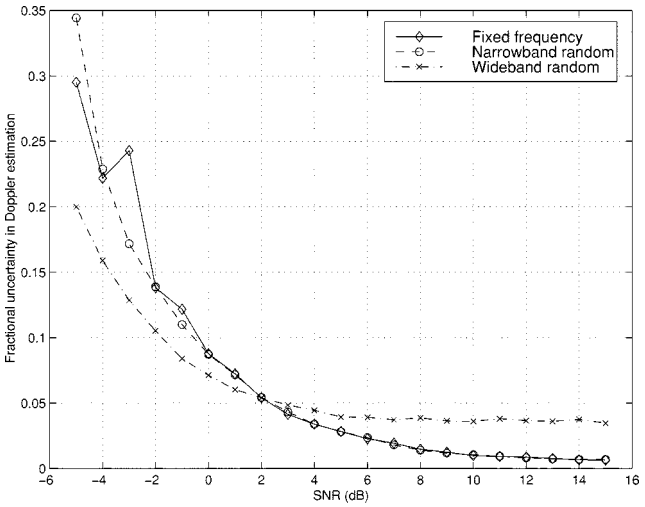

Fig. 12. Fractional uncertainty in Doppler estimation as a function of signal-to-noise ratio (SNR).

VIII. Conclusions

The results described in this paper suggest that the coherent random noise radar technique is useful for estimating Doppler velocities of moving targets. The subclutter visibility, which is primarily limited by the transmitter and receiver local oscillator sidebands [7], will ultimately determine the maximum range at which a target of a certain size and radar cross section can be detected and identified as a moving target. Other sources of phase noise errors such as mixers [8] and I/Q-detectors [9] will also degrade the Doppler performance of the system and these effects need to be quantified in detail. These topics are the subject of ongoing investigations at our end.

Based on our analysis and measurements described in this paper, we are confident that the coherent random noise radar technique has great potential for simultaneous measurement of target range and Doppler due to its near-ideal ambiguity function. The ability to rapidly scan through a range of target delays is restricted by the inability of current photonic delay line technology to provide rapidly switchable delays, but we feel optimistic that this technology will mature in a short time. Another alternative being explored is to reduce the bandwidth to about 500 MHz (consistent with a down-range resolution of 30 cm or 1 ft), and use digital radio frequency memory (DRFM) technology to achieve the delays digitally.

Acknowledgment

The authors would like to thank Dr. W. Miceli, Office of Naval Research (ONR), Arlington, VA, and Dr. V. Chen, Naval Research Laboratory (NRL), Washington, DC, for their useful discussions. They would also like to thank Dr. S. Pappert, Space and Naval Warfare Systems Center (SPAWAR), San Diego, CA, for loan of the photonic delay line used during the field measurments. Thanks are also due to D. Bell, D. Garmatyuk, E. Borissov, and D. Kramer for their assistance during field measurements and data analysis.

References

[1] R. M. Narayanan, Y. Xu, P. D. Hoffmeyer, and J. O. Curtis, "Design, performance, and applications of a coherent ultra-wideband random noise radar," *Opt. Eng.*, vol. 37, no. 6, pp. 1855–1869, June 1998.

[2] W. P. Robins, *Phase Noise in Signal Sources: Theory and Applications*. London, U.K.: Peter Peregrinus, 1982, pp. 203–210.

[3] G. R. Cooper and C. D. McGillem, "Random signal radar, final report," Purdue Univ., West Lafayette, IN, TR-EE67-11, 1967.

[4] J. R. Taylor, *An Introduction to Error Analysis*. Mill Valley, CA: Univ. Sci., 1982.

[5] J. H. Dunn and D. D. Howard, "Radar target amplitude, angle, and Doppler scintillation from analysis of the echo signal propagating in space," *IEEE Trans. Microwave Theory Tech.*, vol. MTT-16, pp. 715–728, Sept. 1968.

[6] D. S. Zrnic, "Simulation of weather-like Doppler spectra and signals," *J. Appl. Meteorol.*, vol. 14, pp. 619–620, 1975.

[7] D. B. Leeson and G. F. Johnson, "Short-term stability for a Doppler radar: Requirements, measurements, and techniques," *Proc. IEEE*, vol. 54, pp. 244–248, Feb. 1966.

[8] C. L. Everett, "Phase noise contamination to doppler spectra," *Microwave J.*, vol. 39, no. 9, p. 105ff, Sept. 1996.

[9] S. J. Goldman, *Phase Noise Analysis in Radar Systems Using Personal Computers*. New York: Wiley, 1989.

Ram M. Narayanan (S'84–M'88–SM'91) received the B.Tech. degree from the Indian Institute of Technology, Madras, India, in 1976, and the Ph.D. degree from the University of Massachusetts, Amherst, in 1988, both in electrical engineering.

From 1976 to 1983, he was a Research and Development Engineer with Bharat Electronics Ltd., Ghaziabad, India, where he was involved in the development of microwave troposcatter communications equipment. He joined the Microwave Remote Sensing Laboratory, University of Massachusetts, Amherst, in 1983 as a Research Assistant. He joined the Electrical Engineering Department at the University of Nebraska-Lincoln, where he is currently a Professor. He currently serves on the editorial board of *Army Battlefield Environment*, a newsletter that is widely distributed to the scientific community within the United States Army. His research interests lie in the area of radar and laser remote sensing of natural surfaces and the development of remote sensing systems for environmental applications.

Dr. Narayanan is active in the IEEE Geoscience and Remote Sensing Society. He served as an invited participant in a National Science Foundation (NSF) workshop on the application of remote sensing technology for monitoring power and dispersed civil infrastructure systems in April 1994. He is also serving on the National Research Council's Committee on Radio Frequencies for the period 1997–2000.

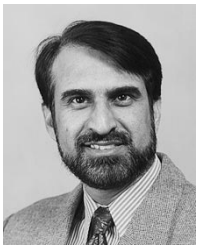

Muhammad Dawood (S'99) received the B.E. degree from NED University of Engineering and Technology, Karachi, Pakistan, in 1985, and the M.S. degree from the University of Nebraska-Lincoln (UNL), in 1998, both in electrical engineering. He is currently working toward the Ph.D. degree at the same university.

In 1996, he joined the Department of Electrical Engineering at UNL, where he is a Research Assistant. Prior to joining UNL, he worked as Research and Project Development Engineer with Pakistan International Airlines (PIA) and as an Instructor of undergraduate classes at the College of Aeronautical Engineering, Pakistan. His research interests lie in the area of radar, wireless communication, and signal processing.